Civil, Architectural and Environmental Engineering Faculty Research & Creative Works

Civil, Architectural and Environmental Engineering

01 Jan 2023

Field Reconnaissance And Observations From The February 6, 2023, Turkey Earthquake Sequence

Gulen Ozkula

Robert K. Dowell

Tugce Baser

Jui Liang Lin

et. al. For a complete list of authors, see https://scholarsmine.mst.edu/civarc_enveng_facwork/2671

Recommended Citation

ORIGINAL PAPER

Field reconnaissance and observations from the February 6, 2023, Turkey earthquake sequence

Gulen Ozkula[1] · Robert K. Dowell[2] · Tugce Baser[3] · Jui-Liang Lin[4] ·
Ozgun A. Numanoglu[5] · Okan Ilhan[6] · C. Guney Olgun[7] · Cheng-Wei Huang[4] ·
Tunc Deniz Uludag[8]

Abstract

On February 6, 2023, a sequence of earthquakes hit Kahramanmaras, Turkey, with magnitudes of $M_w = 7.8$ and 7.5, at 4:17 am and 1:24 pm local time, respectively. According to the records, the $M_w = 7.8$ event was the biggest earthquake since the 1939 Erzincan earthquake of the same magnitude and second-strongest recorded after the 1668 North Anatolia Earthquake. However, it was the most devastating earthquake in the history of Turkey in terms of structural and geotechnical damage and fatalities caused by this. The objective of this article is to explore the aftermath of this major seismic event, with a particular focus on the following areas: (1) regional geology and seismotectonics background, along with geological field observations; (2) seismological context and analysis of strong ground motion records; (3) a summary of field reconnaissance findings; (4) an evaluation of residential structures, bridges, schools, hospitals, and places of worship, as well as, building foundations; (5) a study of soil and rock slopes, seismic soil liquefaction manifestations, rockfalls, earth dams, harbors, lifelines, ports, deep excavations, and retaining structures. The conclusions drawn herein are from the field reconnaissance and, therefore, are preliminary in nature. Subsequent research utilizing the gathered data will offer more comprehensive insights and definitive conclusions regarding the observations discussed.

Keywords Turkey earthquake · Geostructures · Residential buildings · Bridges · Earthquake reconnaissance

1 Introduction

On February 6, 2023, a M_w 7.8 earthquake occurred at 4:17 am (local time) in southern Turkey followed by a M_w 7.5 earthquake in the same general region about 9 h later, at 1:24 pm (local time). The epicenter of the M_w 7.8 earthquake was located at 37.288°N, and 37.043°E with a focal depth of 10 km (USGS 2023a), while the epicenter of the M_w 7.5 earthquake was approximately 175 km from the first event (38.089°N, and 37.239°E) with a focal depth 10 km. As a result of this unprecedented series of back-to-back earthquakes, in populated regions, damage was observed for residential buildings, industrial structures,

bridges, transportation systems, earth structures, harbors and lifelines, with direct infrastructure loss exceeding \$34 billion according to initial estimates (World Bank, 2023). In addition to strong ground sharing in the near field, one of the root causes that exacerbated this natural hazard into a catastrophic disaster was the large ground deformations such as landslides, fault rupture, and ground subsidence, which severely affected critical infrastructure including lifelines and roads. The cities affected most by strong ground shaking are Kahramanmaras, Adiyaman, Hatay, Osmaniye, Gaziantep, Malatya, Adana, Diyarbakir, Elazig and Kilis with residents of over 15 million (which constitute about 17% of Turkey's population). According to official records, the number of fatalities was about 50,000 and more than 100,000 people were injured. A total of 19,284 buildings in ten different cities collapsed and 373,038 buildings were reported as damaged to different levels (Ministry of Environment, Urbanization and Climate Change, 2023).

The reconnaissance team arrived to the region on February 11, one week after the occurrence of the sequential events and visited towns and cities, including Iskenderun, Antakya, Osmaniye, Kahramanmaras, Gaziantep, Nurdagi, Golbasi and Antakya, to collect and document perishable data in the form of structural damage and geotechnical effects. More specifically, the subsequent investigative efforts have mostly focused on documenting the following: background information related to the geology and seismotectonics of the region and geological field observations, seismological background and processing of strong ground motion records, brief field reconnaissance information, the performance of residential structures, the performance of bridges, performance of building foundations, information on soil and rock slopes, seismic soil liquefaction manifestations, rockfalls, earth dams, harbors, lifelines, ports, deep excavations, retaining structures, industrial structures. It is important to note that the authors' conclusions are preliminary. Future research on the collected data will provide greater insight, as well as more definitive conclusions on the presented observations.

2 Strong ground motion characteristics

The East Anatolian Fault Zone (EAFZ) is known to be seismically active due to its extrusion between stable Eurasian and Arabian plates, where the latter moves towards the northeast relative to the Anatolian plate (Cetin et al. 2023), leading to a horizontal slip rate of 10–11 mm/year in the EAFZ (Cetin et al. 2003). Considering this movement, many historical records that describe the events and damaged areas such as the earthquakes that occurred on 1114, 1138, 1269, 1344, 1514, 1544, 1795 (Şeşetyan et al., 2023) and the Elazig earthquake on January 24, 2020 with $M_w = 6.8$ (https://tadas.afad.gov.tr/event-detail/8071) lend credence to the potential of the EAFZ to produce large magnitude events. On February 6, 2023, at 04:17 am local time, an earthquake with epicenter at 37.225°N 37.021°E (26 km east-northeast of Nurdagi, Gaziantep), with moment magnitude (M_w) of 7.8, and depth of 10.0 km struck Turkey (USGS, 2023a). Figure 1 illustrates the ruptured fault (in red), which is composed of Erkenek, Pazarcik and Amanos fragments of EAFZ and produced a strike–slip movement with a length of 290 km (Hancilar et al. 2023), resulting in the M_w 7.8 earthquake. The bilateral fault rupture initiated in the Narli fault and is followed by a slip from Pazarcik to Erkenek in the northeast direction, as well as slip throughout the Amanos segment towards the southwest direction, after some delay (Cetin et al. 2003).
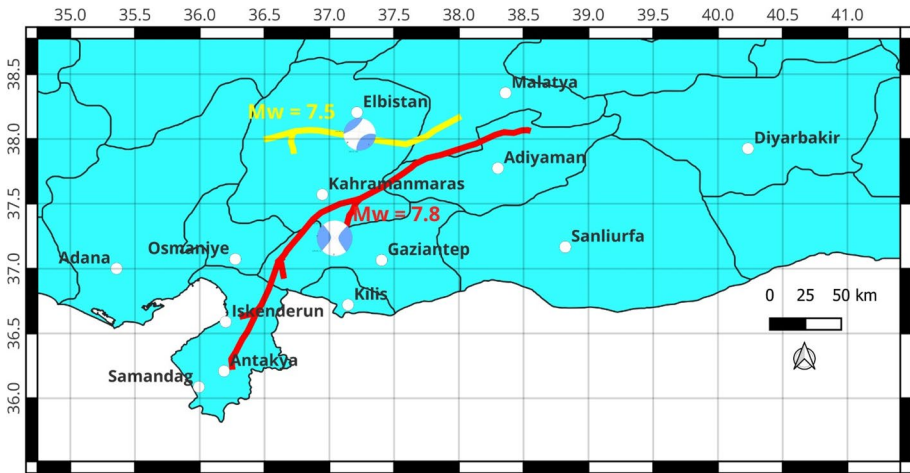
Fig. 1 The fault ruptures and epicenter locations of $M_w = 7.8$ and $M_w = 7.5$ (The beach ball diagrams representing the focal mechanism were downloaded from USGS (2023a) and USGS (2023b), and the fault locations were approximately digitized from SiteEye)

After ~9 h from the first event (February 6, 2023, at 1:24 pm local time), an earthquake with epicenter at 38.024°N 37.203°E (4 km south–southeast of Ekinozu, Kahramanmaras), with M_w of 7.5 and depth of 10 km shook the area (USGS, 2023b). Analogous to the M_w 7.8 earthquake, the moment tensor solution exhibited in Fig. 1 indicates a strike–slip movement consistent with the EAFZ fault mechanism. Cetin et al. (2003) estimated a 160-km rupture length from Cardak fault towards Dogansehir (Malatya) fault zone with observed surface displacements ranging from 2 to 8 m.

2.1 Strong ground motion data process

The M_w 7.8 and M_w 7.5 events were recorded at 290 and 267 stations of AFAD (Disaster and Emergency Presidency of Turkey), respectively. All of these motions were downloaded as raw acceleration data to compare with the design spectra required by the Turkish Earthquake Building Code (TEBC 2019) and were subjected to a visual check to detect long-period noise (≤ 0.1 Hz), which can be identified through (i) velocities that do not approach the value of zero at the end of the record (Akkar and Boore 2009), or (ii) displacement time-histories which exhibit wobbles or significant shifts from the zero baseline. Figure 2 illustrates the raw acceleration time-history (TH) recorded by Station 3802 during the M_w 7.5 event. The wavering observed in the velocity TH calculated through cumulative summation of acceleration TH indicates the long-period noise in raw acceleration data, leading to larger and fictitious values in displacement TH.

This baseline shift of the raw acceleration data was resolved through the ground motion processing approach of BAP (Basic Strong-Motion Accelerogram Processing Software), which is proposed in Converse and Brady (1992) and is implemented in DEEPSOIL V7.0 (Hashash et al. 2020) through the "Baseline Correction" option in DEEPSOIL v7.0. Figure 2 presents the application of baseline correction to raw
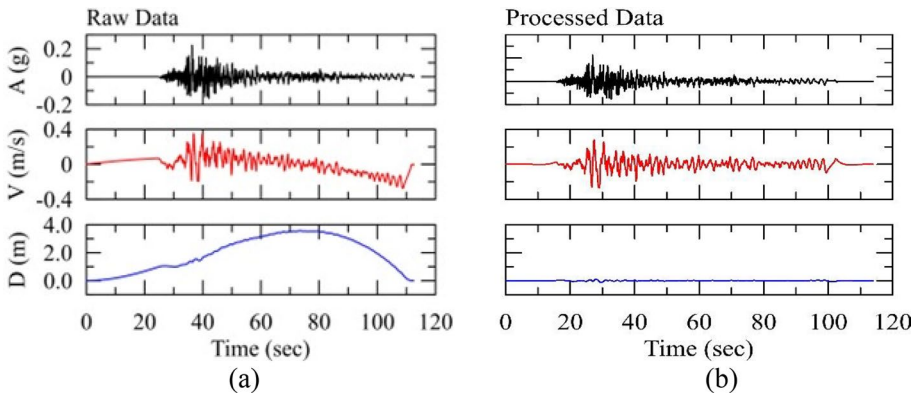
Fig. 2 Acceleration (A), velocity (V) and displacement (D) time histories recorded by station 3802 during $M_w = 7.5$ earthquake, **a** raw, **b** processed

acceleration data in that (a) the downward slope and offset in velocity TH in Fig. 2a are removed and b the fictitious displacement trend in Fig. 2a is corrected in Fig. 2b.

2.2 Comparison of spectral curves at selected stations with TEBC (2019) design spectrum

Figure 3 shows the recorded THs and compares the spectral acceleration plots with the design spectra required by the Turkish Earthquake Building Code (TEBC 2019) for return periods of 475 years (10% probability of exceedance in 50 years) and 2475 years (2% probability of exceedance in 50 years) for rock-like material ($V_{S30} > \sim 600$–700 m/s) and soil sites for the M_w 7.8 event. PGA values recorded at Station 4611 ($V_{S30} = 731$ m/s and rupture distance (R_{RUP}) of 16.9 km) located in the city of Kahramanmaras are 0.32 g and 0.35 g for E–W and N–S components, respectively. Spectral acceleration (SA) plots of the two horizontal components are consistent with the 475-year design spectrum from the TEBC (2019). In the case of Station 4616 located at a soil site ($V_{S30} = 390$ m/s and $R_{RUP} = 2.34$ km) in Kahramanmaras, recorded PGAs for E–W and N–S components increase to 0.51 g and 0.67 g, respectively, compared to Station 4611, and the spectral curves of recorded ground motions at Station 4616 reach the TEBC (2019)-2475 years spectrum at oscillator periods (T_{OSC}) of ~ 0.5 s, ~ 0.75 s and 1.5 s. This condition is known to occur due to site effects from strong ground motion (Seed et al. 1988) and is more pronounced for the city of Hatay than at other locations, where SA values from Station 3135 ($V_{S30} = 460$ m/s and $R_{RUP} = 34.21$ km) exceed the TEBC (2019)-2475 years spectrum for $T_{OSC} \leq 1.0$ s, but SAs of motions recorded at Station 3116 ($V_{S30} = 870$ m/s and $R_{RUP} = 17.43$ km) are on the order of TEBC (2019)-475 years spectrum. The analogous evaluation to that described above is performed using the recorded motions from two stations in Kayseri during the M_w 7.5 event, as illustrated in Fig. 4. Even though the SA motion values at Station 3804 ($V_{S30} = 637$ m/s, $R_{RUP} = 77.77$ km) lie notably beneath the TEBC (2019)-475 years spectrum, Station 3802 ($V_{S30} = 305$ m/s, $R_{RUP} = 49.33$ km) is thought to have significant site amplification, leading to the exceedance of SA values for the E-W component to the TEBC (2019)-2475 years spectrum for 2.0 s $\leq T_{OSC} \leq 2.5$ s.

Fig. 3 The baseline-corrected acceleration (A) time histories, response spectral accelerations (SA) for E–W and N–S components and design spectra suggested by TEBC (2019) for return periods of 2475 years and 475 years for Station 4611 located in Kahramanmaras. The same information is presented Station (Kahramanmaras) 4616, Station (Hatay) 3116, and station (Hatay) 3135 for M_w= 7.8 event
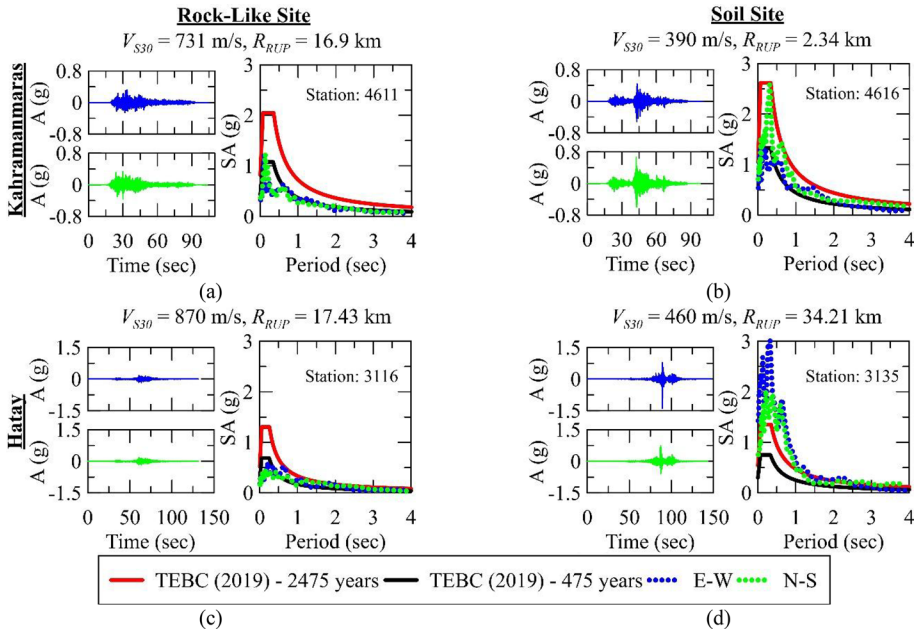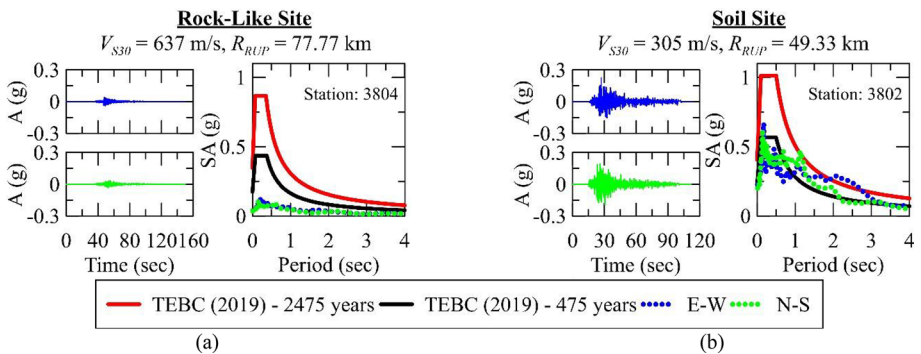

Fig. 4 The baseline-corrected acceleration (A) time histories; response spectral accelerations (SA) for E–W and N–S components and design spectra suggested by TEBC (2019) for return periods of 2475 years and 475 years for Station 3804 located in Hatay. The same information is presented for station (Kayseri) 3802 for Mw = 7.5 event

3 Geotechnical findings and performance of geostructures

3.1 Overview

Two events and aftershocks impacted several provinces in the southeast of Turkey and

caused geotechnical engineering issues. The team performed a reconnaissance mission to document geotechnical engineering-related problems and to collect perishable data pertaining to the geostructures in the region immediately after the earthquakes. This section focuses on the preliminary investigations of the geotechnical aspects, including earthquake-induced liquefaction manifestations, settlements, slope, and earth dam deformations and instabilities. An overview of the locations where geo-tagged data were found (pictures, measurements, drone footages, etc.) and area coverage are given in Fig. 5.

3.2 Seismic soil liquefaction

Widespread seismic-induced liquefaction was found in the Iskenderun district of Hatay. Iskenderun is nestled on the southern Mediterranean coast along the foothills of the Amanos Mountains and stretches for about five kilometers. The coastal areas of Iskenderun are underlain by young marine deposits and artificial fill. There are also several creeks originating from the Amanos Mountains towards the bay, and these have contributed to the local soil formations. Young marine deposits and fills dominate the coastal plains covering part of the older sections of Iskenderun until the town transitions into higher ground towards the foothills of the mountainous terrain. The soils along the coastal area include loose-to-medium dense sands and silty sands with variable thickness depending on the proximity to the coastline. Soil conditions are highly variable because of the marine and alluvial depositional environment, as well as the reclamation fill. Most of the buildings are on shallow mat foundations, and there are also high-rise structures on deep foundations with jet grout columns.

Preliminary observations indicate that Iskenderun experienced widespread liquefaction and lateral spreading. The observations regarding liquefaction, liquefaction-induced lateral spreading and ground deformations, and seismic-induced deformations in different parts of Iskenderun are presented in Fig. 6 through Fig. 8. Settlements were observed both in near-free-field conditions (Fig. 7) and under the structures, including the public dock of Iskenderun (Fig. 8). Evidence of soil ejecta and significant settlements was observed around a multi-story building and a mosque built on a reclamation area (Fig. 6). Settlements were

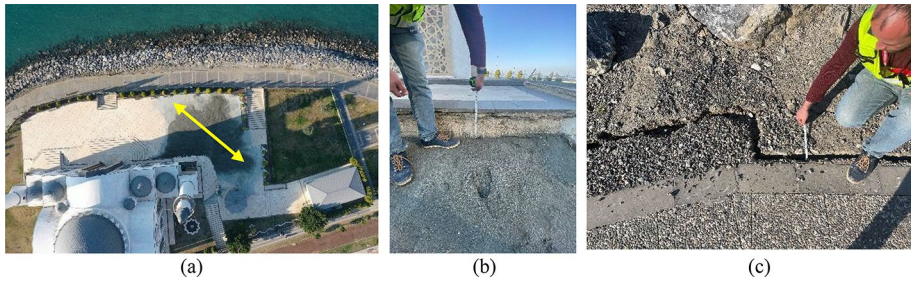**Fig. 5** Plan-view of the geotechnical reconnaissance and covered areas

Fig. 6 Liquefaction manifestations in Nihal Atakas Mosque (~36°35′35.27"N/36° 9′26.74"E): **a** bird's-eye view of the sand ejecta at the corner; **b** up to 30-cm settlements of the sand near the mosque; **c** lateral spreading near the mosque towards the sea
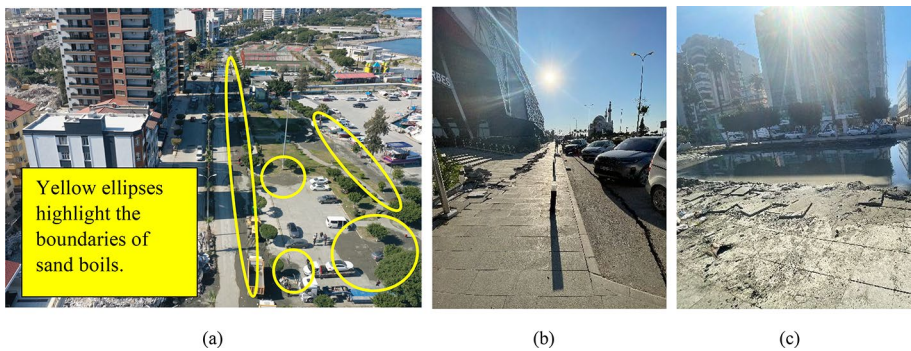

Fig. 7 Liquefaction manifestations (sand boils) **a** on Ataturk Boulevard (~36°35′26.86"N/36° 10′40.39"E); **b** cracks formed due to lateral deformation near Forbes shopping center (~36°35′36.52"N/36° 9′34.67"E); **c** near tennis courts (~36°35′26.95"N/ 36° 10′28.39"E): water accumulation and sand boils on the street

Fig. 8 Ground settlements and lateral deformations on Iskenderun dock (~36°35′40.67"N/36° 10′38.69"E): **a** ground subsidence at the pier and the lighthouse; **b** ground subsidence at the dock; **c** free field sand boils at the port

observed to be between 5 and 30 cm under the multi-story building, whereas settlements at the public dock reached values as high as 150 cm (Fig. 8).

Liquefaction was most likely triggered due to marine sediments and reclamation fill that underlie the coastal Iskenderun town. Sands and silty sands are prevalent within the area that suffered liquefaction-induced ground failure. Liquefaction was evident from ground cracks, sand boils, apparent subsidence, and lateral spread, as well as the settlement of

buildings on shallow foundations. It is estimated that the waterfront area settled by about 50–60 cm and the buildings on mat foundations in this area settled by about 5–50 cm. Ground subsidence as high as 150 cm was observed at the Iskenderun dock situated at the northern end of Iskenderun. It was also observed that the severity and magnitude of liquefaction-related ground failure gradually diminished by about 400–500 m inland from the waterfront. This transition can be attributed to the decreasing thickness of the liquefiable deposits inland from the waterfront. It was observed that buildings and structures founded on deep foundations with jet grout columns performed well, without any catastrophic failure.

3.3 Dams

Several earthquake-induced damages were observed at the Kartalkaya Dam in Kahramanmaras and the Ariklikas Dam in Osmaniye. The Kartalkaya is one of the most important dams in the region, as it has been supplying irrigation water to Pazarcik County and tap water to the city of Gaziantep. The dam was built on the Aksu River for irrigation and for flood prevention for the town of Pazarcik. The Kartalkaya Dam has a crest elevation of 720 m and catchment elevation ranging between 680 and 2470 m. It has been in operation since 1971 with a reservoir area of 11 km^2 and a drainage area of 1088 km^2 that can supply irrigation water to 200,000 acres of farmland. During the construction phase, the capacity was calculated as 200,000,000 m^3, but current capacity has decreased to 160,000,000 m^3 because of the sediment fill in the reservoir. The sediment fill caused by rainfall-induced erosion has led to several studies focusing on erosion in the area (Yuksel et al. 2008; Taskesen Ozturk, 2018). Significant damages on the crest and right-wing of the Kartalkaya Dam are shown in Fig. 9, which are associated with the combined effect of seismic load-induced cracks and lateral displacements at the central part of the crest, and rockfalls of the upstream part of the dam. The cracks are longitudinal to the dam crest, with dimensions of twenty meters long and having a depth of 0.5 m and width of 0.3 m. No significant orthogonal cracks were observed in the crest. There was no upstream or downstream damage observed at the side slopes. The reservoir had already been almost empty due to the present climate, and there was no leakage through the gates. Wings located at the water inlet through the gates have damage due to intense shaking. One segment moved toward the earth dam, where seismic compression occurred. Besides there are no connections between segments on the wings so that damaged segments easily move apart.

The Ariklikas Dam is a homogeneous earth dam constructed between 1994 and 1998 in Osmaniye for irrigation purposes. The crest height from the stream level is almost 32 m. Cracks formed during the earthquakes at the crest level, with crack widths ranging from 2.2 m to 4.0 m. The lateral movement is toward the upstream. No damage was observed on hydraulic structures, except for minor cracks on the curtain walls of the spillway. In addition, the face of the dam at the upstream side was observed to be significantly settled close to the crest and bulged out towards the toe of the dam, with a visible opening at the center of the slope. The details of the slope instability and information of the dam are given in Fig. 10a, b, respectively.

The Yarseli Dam is an earth dam constructed between 1985 and 1991 in Antakya for irrigation purposes. The crest height from the stream level is almost 37 m as seen in Fig. 11a. Crest cracking with lateral displacements varies between 0.15 and 0.25 m as shown in Fig. 11b. There were no sand boils on the earth-dam surface, so no trace of liquefaction was observed. The hydraulic structures had no obvious cracking or damage.

Fig. 9 Deformations observed on the Kartalkaya dam (~37°28′06.01"N/37°14′20.14"E): **a** compression cracks and lateral displacements at the crest of Kartalkaya dam; **b** longitudinal cracks in the middle of the crest; **c** moved segment and compression; **d** earthquake-induced rock fall and associated cracks on the crest

Fig. 10 Deformations observed on the Ariklikas (~37°09′25.70"N/36°30′55.96"E) dams: **a** Ariklikas Dam (side view); **b** Ariklikas dam construction details (in Turkish)

3.4 Landslides

One of the largest-scale geotechnical engineering problems in the earthquake-affected areas is the massive landslide in the Tepehan village near Hatay, Turkey, that occurred after the earthquake sequence. Aerial footage taken in the area shows the canyon-like terrain after the earthquake created very large cracks, having dimensions of 300 m × 200 m × 30 m. The aerial picture of the landslide is given in Fig. 12a, b. The geology of the area was investigated by Selcuk (1985), and it revealed a Middle Miocene-aged Tepehan

Fig. 11 Aerial pictures of the Yarseli dam (36.194290N, 36.329264E): **a** Overview; **b** Cracks in the crest

Fig. 12 Landslide at an olive farm near Turkey-Syria border (Altinozu, Hatay): **a** main crack (bird's-eye view) at ~36°09′42.41"N/36°13′13.40"E; **b** main crack–near-front view of the crack; **c** potential landslide origin and tension cracks at 36°09′28.18"N/36°13′00.65"E **d** displaced single family home in Tepehan village

formation, which consists of sandstone, clayey limestone, claystone, and marl. Sandstones are usually medium-thick bedded loosely packed and contain a significant amount of thin fossil shells that are prone to breakage. Similar to the sandstones, clayey limestone contains mollusk shells.

The slope of the landslide ranges from 15 to 25 degrees, steepening towards the toe. The area had been particularly dry for several years, and there is a potential for causing extensive desiccation cracks. There was a heavy rainfall that lasted for several days preceding the earthquakes, inundating and saturating the dry soil through the cracks.
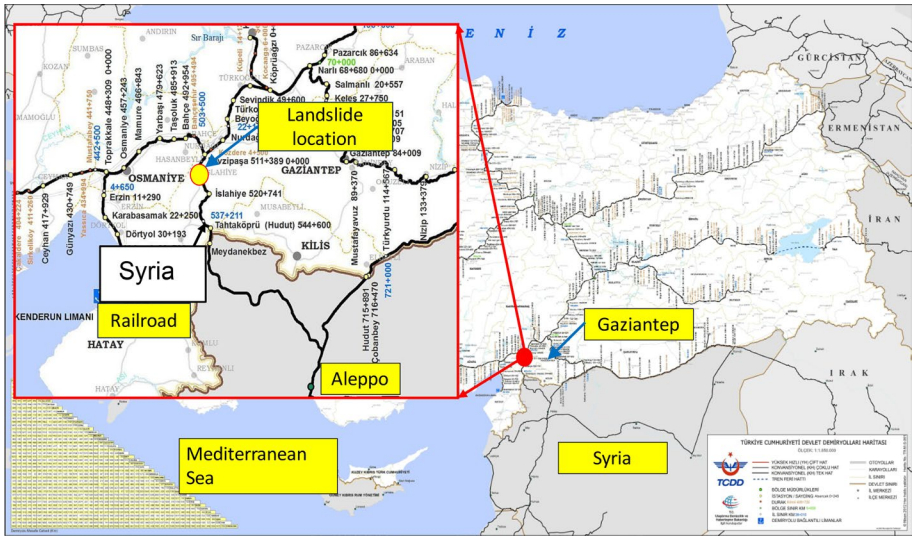
Fig. 13 Overview of the railroad map of Turkiye–Syria (obtained from rayhaber.com) and landslide location (~37°06′43.41"N/36° 39′34.91"E)
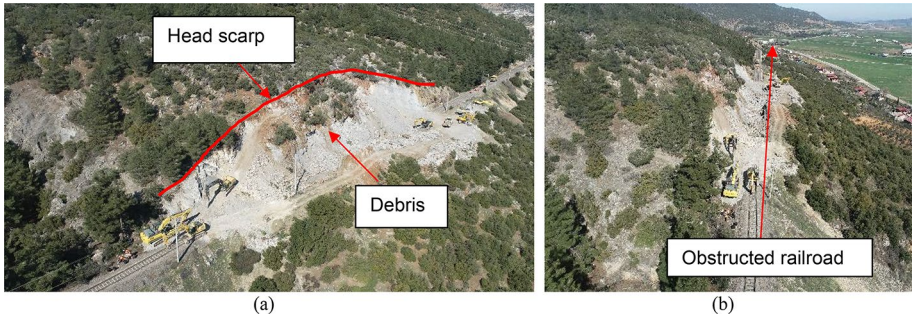
Fig. 14 Landslide near a railroad in Islahiye at~37°06′43.41"N/36° 39′34.91"E (aerial photographs taken for the same slope failure at different angles)

The massive landslide followed the earthquakes, triggering a mass movement of several cubic meters of soil and rock debris. This landslide might further mobilize due to rainfalls and creep. The team found the potential origin of the landslide, which was manifested with tension cracks approximately 300 m above the head scarp (Fig. 12c, d).

Another landslide was documented in the Fevzipaşa–Meydanekbez segment running N-S from the main Adana-Gaziantep rail line towards Aleppo, Syria. The approximate location of the landslide is marked in Fig. 13. As can be seen in the map, this is a critical location and is one of the segments connecting Syria with Turkey. The collected data are not enough to report if the landslide was caused by the first or second earthquake in the sequence. Aerial footage of the landslide indicates that the head scarp is approximately 100 m long (Fig. 14a). Several backhoes were immediately sent to the site for debris removal as can be seen in Fig. 14b.

Fig. 15 **a** Demolition work, **b** an excavator pulling down damaged buildings, **c** the damage states of buildings possibly contaminated by demolition work

Table 1 Structural damage levels in cities by percentage (%) (MEUT Report, 2023)

City	Damage level					
	None	Slightly	Others	Extensive	Par. Collapse	Full collapse
Adana	72.11	21.71	5.51	0.51	0.05	0.12
Adiyaman	29.9	32.54	14.58	15.9	1.85	5.23
Diyarbakir	59.79	24.2	13.55	1.85	0.14	0.47
Gaziantep	59.7	18.27	15.42	4.35	0.71	1.55
Hatay	49.47	23.54	7	13.36	2.31	4.32
Kahramanmaras	37.75	28.69	14.75	12.43	2.66	3.72
Kilis	50.39	31.39	9.31	5.83	0.78	2.29
Malatya	26.12	26.89	20.65	21.57	0.63	4.13
Osmaniye	63.98	20.98	8.34	5.66	0.58	0.46
Sanliurfa	49	34.85	15.16	0.78	0.09	1.3

4 Performance of residential structures

The structural reconnaissance team visited the region affected by the earthquake sequence on February 20, i.e., two weeks after the earthquakes. It was observed that demolition work had started before the reconnaissance (Fig. 15a), i.e., some heavy machines, such as excavators with buckets or claws, had pulled down some damaged buildings, as shown in Fig. 15b. An effort was made to exclude the damage states of buildings that were possibly exacerbated by demolition work (Fig. 15c) as noted by discussion with local authorities. Overall, the observations were in agreement with reported condition assessments conducted by the Ministry of Environment and Urbanization of Turkey (MEUT) on 736,851 buildings in the effected region. Collected data show that a total of 19,284 buildings collapsed from the earthquake sequence and almost half of the investigated buildings (373,038) were damaged to varying levels as shown in Table 1.

4.1 Reinforced concrete (RC) building

4.1.1 Construction and materials

Figure 16a, b reveals two different construction practices in Turkey. By observing the forms and scaffolding, Fig. 16a indicates that the fresh concrete of columns, beams, and slabs of a story was cast as a whole. In contrast, Fig. 16b indicates that the fresh concrete of columns was cast first and then followed by casting the fresh concrete for beams and slabs. The integrity of the building using the former approach (Fig. 16a) should outperform that of the latter (Fig. 16b). Moreover, Fig. 16c shows an existing two-story building with an additional third story. Because the dead load of the building was amplified approximately 1.5 times, it would have certainly increased the seismic risk of that building if the existing two stories were not adequately strengthened. Figure 16d shows that instead of deformed rebar, plain reinforcement was used, and, as a result, bond between rebar and concrete was poor. In addition, the spacing of stirrups was large at approximately 30 to 40 cm, with coarse aggregates seeming to be too small (Fig. 16d) since these buildings were designed by using the old seismic code. Figure 16e, f shows that there is no separation between buildings. In other words, seismic damage resulting from pounding between buildings likely occurred.

4.1.2 Collapsed buildings

In terms of the appearance of building collapse, it is straightforward to categorize them into "lie-down", "sit-down", and "knee-down" types (Lin et al. 2020). The occupants of lie-down collapsed buildings have almost no chance of survival, which usually causes the most fatalities during seismic events. The sit-down and knee-down collapsed buildings only directly threaten the lives of occupants of fully or partially collapsed stories, rather than all stories. Figure 17a, b shows lie-down collapsed buildings, one of which was still under construction, with its sale advertisement nearby (Fig. 17a), while the other building

| (a) | (b) | (c) |
| (d) | (e) | (f) |

Fig. 16 **a** and **b** Two buildings with different construction practices, **c** a building with an added third story, **d** poor concrete and plain reinforcement, **e** and **f** no separation between buildings

Fig. 17 **a** and **b** lie-down collapsed buildings, **c** a building with pancaked third story, **d** and **e** three similar buildings with different damage states, **f** close-up photograph of the first story of the right building, **g** bi-directional and one-directional plastic hinges, **h** and **i** a knee-down collapsed building

was occupied, as shown in Fig. 17b. If the lateral force-resisting system of the building shown in Fig. 17a had been completed before the earthquake, the soft-and-weak lower story of the building could be attributed to either design or construction issues, rather than the possibility of the building being remodeled by occupants. Figure 17c shows a sit-down collapsed six-story building with a pancaked third story, which is also called a soft story. Figure 17d shows three similar eight-story buildings with different damage levels. The left building partially pancaked at the second, third, and top stories (Fig. 17e), but the other two buildings were only moderately damaged. This observation implies that the lateral force-resisting elements on the front side of the second and/or third stories of the left building probably had been remodeled before the earthquake, which resulted in the weak second and/or third stories.

The far-right building in Fig. 17d has a masonry wall at the first story so its damage was less than that observed in the mid building. The wall showed shear failure with two major diagonal cracks at angles of 45° and 60° (Fig. 17f). Additionally, bi-directional and one-directional plastic hinges were successfully formed at the bottom ends of the first story columns (Fig. 17g). The bi-directional plastic hinge indicates that the building suffered significant ground motion in both mutually perpendicular horizontal directions. Because strength deterioration of a column in one direction affects the performance of the column in the other direction, three-dimensional analysis and design of buildings should be

stressed in the future. Figure 17h, i shows a knee-down collapsed building, in which the beams were separated from the columns and walls. By observing the almost intact surface of the beam bottom, it indicates that the beams were inadequately connected not only with the walls, but also with the columns. Furthermore, by observing the relatively separated locations between the beams and columns of the first story, this building was likely displaced rightward and inward of the photograph. That is to say, the building experienced rotational displacement demands in plan view (twisting) under the earthquake. Some buildings collapsed or were damaged by issues (e.g., soil liquefaction) other than structural. Figure 18a, b illustrates an overturned building and unequal settlement of a building, both with good structural integrity. Figure 18c, d shows ground settlement, surface cracking, and sand boils, which indicate soil liquefaction in that area. Secondary disaster caused by the earthquake was also noticed; Fig. 18e shows a building, in which damage caused by fire is perhaps more serious than that caused by the earthquake shaking. Figure 18f indicates a slightly-to-moderately damaged five-story building with some damaged facilities (e.g., water tanks) at top the roof. Although the building was successful against the seismic strike, damage of nonstructural components certainly affected the function of the building.

4.1.3 Structural members

Figure 19a and b shows that two buildings collapsed along the street because the weak direction of columns was oriented along the street. The large aspect ratio of column cross sections, rather than a square, seems to be common in the region that was observed to increase indoor space. Nevertheless, once all columns are oriented in the same way, the building would be soft and weak in the weak-axis direction of the column, i.e., the vulnerable direction of the building to earthquakes. In addition, the strong beam-weak column concept likely exists in the weak direction [i.e., plastic hinges will be formed in columns rather than in the beams, such as that shown in Fig. 19c]. Figure 19d shows the

(a) (b) (c)

(d) (e) (f)

Fig. 18 **a** An overturned building, **b** unequal settlement of a building, **c** settlement of ground, **d** sand boils, **e** secondary disaster, **f** damaged facilities atop a roof

Fig. 19 Structural damages **a** and **b** collapsed buildings along a significantly weak direction; **c** plastic hinges at top and **d** plastic hinges at bottom of columns, **e** an almost intact building, and **f** a close-up photograph of **e**

weak-direction plastic hinges at the bottom ends of the columns. Additionally, the spacing of stirrups within the plastic hinge zones was greater than 20 cm. Figure 19e, f shows an almost intact five-story building. The close-up photograph of the first story indicates that the orientation of columns is not the same (i.e., some columns are rotated 90° in relation to the other columns). Note that while arranging the orientation of columns with large aspect ratios, not only the overall stiffness of columns in each horizontal direction, but also the plan distribution of columns, should be carefully considered. Otherwise, buildings are possibly plan-asymmetric, i.e., they will simultaneously translate and rotate in plan view from ground motions.

Figure 20a shows two buildings at one construction project. The progress of the right building was ahead of that of the left building. Figure 20a shows that the exterior and partition walls (often called infill walls) are usually made of bricks, which are erected after completing the beam-column frame system. The thickness of typical brick walls is 15 cm, which consists of 10 cm thickness of bricks and 2.5 cm covering on both sides of the bricks (Fig. 20b). Because there are no connectors between the brick walls and beams/columns, the brick walls fall out of the beam-column frames (Fig. 20c–e). At this point, it is not clear if the infill walls are considered in the structural analysis and design of the buildings in Turkey. Nevertheless, Fig. 20f shows that the infill walls indeed share the seismic force and partially support the building weight. Beams and columns were thus protected from damage to a certain extent (Fig. 20f). However, the participation of infill walls in the lateral force resistance significantly increases the lateral stiffness of beam-column frames. Therefore, the actual vibration periods of buildings with infill walls are substantially less than those obtained from numerical models without considering infill walls. In other words, the actual sustained seismic force of buildings is probably greater than the design base shear obtained from the numerical models without considering infill walls. Also infill walls falling to the streets represent a severe hazard to people. Turkey should decide to either consider infill walls in the seismic performance or not. These walls should be connected properly to the RC frame members and bricks or blocks properly connected to each other. If the

Fig. 20 **a** Two buildings of one construction project, **b** a typical brick, **c** and **d** brick walls popped out of frames, **e** brick walls fallen down, **f** beams and columns were almost intact but brick walls seriously cracked

infill walls are not to be considered for the seismic resistance, then gaps should be provided between the walls and frame members.

The floor slab systems used in Turkey seem to be categorized into two types: one type is supported by beams and columns (Fig. 21a) and the other type is supported by only columns which can be called hidden beam slabs [i.e., no beams, as shown in Fig. 21b]. The hidden beam slab usually consists of a flat slab that is reinforced with steel bars and has a shallow beam integrated into it. The beam is usually placed at the perimeter of the slab and
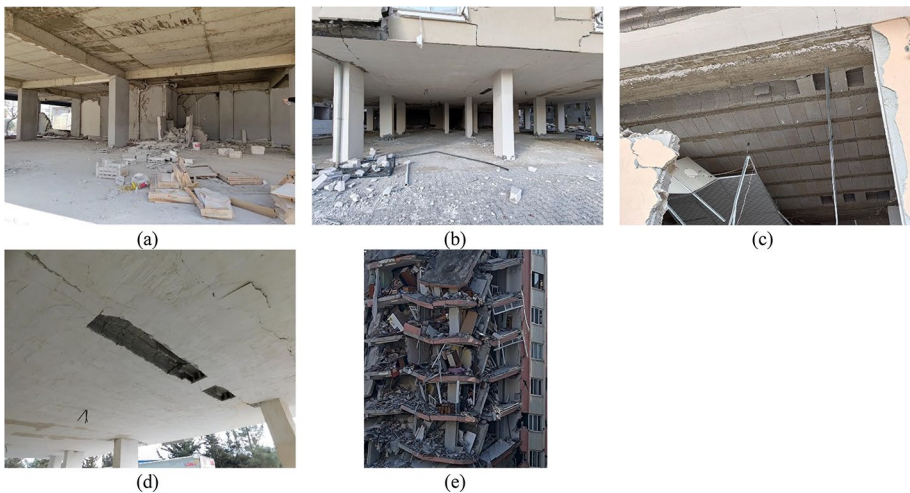

Fig. 21 A floor slab system **a** supported by beams and columns, **b** directly supported by columns, **c** and **d** bricks of the no-beam slab system fallen down, **e** a building with the no-beam slab system was under demolition

is surrounded by the concrete slab. The beam and slab work together to transfer loads from the structure above to the supporting columns or walls. However, it was observed that these slabs are made of bricks, whereas the bricks are possibly fallen down from earthquakes, as shown in Fig. 21c, d. In light of some collapsed or seriously damaged buildings consisting of that floor slab system [e.g., Figs. 17b and 21e, which is a close-up photograph of the left building shown in Fig. 15c], the seismic performance of the no-beam slab system is certainly in doubt.

In Turkey, close and open overhangs are commonly used in building design, such as balconies, semi-balconies, and extended rooms. However, previous earthquakes have shown that buildings with overhangs tend to sustain more damage compared to those without. Despite that the Turkish seismic design code allows for overhangs and requires them to be designed to withstand seismic loads, numerous issues have been reported during construction in post-earthquake assessments (GEER 2020, DAUM 2020, METU-EERC, 2011). Damage examples caused by overhanging structures are shown in Fig. 22a. High stress is place on the columns at cantilever beam connections that intersect with overhangs, leading to significant structural damage at these critical locations. To increase rigidity at these junctions, it may be advisable to use reinforced concrete walls instead of columns if overhangs are unavoidable. A common type of column damage occurs when the columns are partially restricted from lateral movement by strong infill walls or nonstructural partitions of partial heights. These captive columns are prevalent in many buildings, often found in areas such as staircases, toilets, and rooms with windows, primarily because structural engineers do not typically consider them in their earthquake-resistant designs. As shown in Fig. 22b, these captive columns can sustain significant damage during earthquakes. Additionally, it has been demonstrated that equations provided in the main design codes, such as ACI 318 (2005), cannot accurately predict their shear capacity, with the difference sometimes exceeding 150%. Consequently, their existence in buildings should be avoided.

4.2 Masonry buildings

Masonry buildings were generally located in rural areas of the seismic disaster regions. Figure 23a, b shows that two old masonry buildings made of clay bricks were essentially intact, or slightly damaged, despite the two buildings seeming to be not engineered

Fig. 22 Residential building damages **a** due to overhangs, **b** captive/short column due to strong infill walls

Fig. 23 a–c Essentially intact or slightly damaged masonry buildings, **d** and **e** moderately damaged masonry buildings, **f–h** severely damaged masonry buildings, **i** a pure sliding mode of failure mechanism of a brick wall

structures. The masonry walls and tiled roof stayed with structural integrity from the earthquake. Note that the water tanks atop the roofs still remained, i.e., no damage to the supports of the water tanks. Because one-story masonry buildings are very stiff, ground accelerations are not amplified much at the roof line. In contrast, some similar water tanks on top of mid-rise and low-rise buildings in urban areas were toppled down (Fig. 18f). This observation means that whether the supports of water tanks are strong enough depends on the roof acceleration demands, which are usually greater as the number of stories increases. Figure 23c shows a relatively new stone masonry structure, which also seemed to be intact following the earthquake. Figure 23d, e shows moderately damaged masonry buildings with a few fallen bricks and diagonal shear cracks on the walls. Figure 23f, g illustrates severely damaged masonry buildings with crushed or toppled brick walls at the corners. This observation indicates that the brick walls subjected to bi-directional forces are a specific vulnerability of masonry buildings. Lack of connection between orthogonal walls in masonry structures may cause damage if these walls do not share some bricks to act together as shown in Fig. 23f, which was made of two-leaf brick walls. In light of the different damaged heights between the two leaves of brick walls, the mortar between the multi-leaf brick walls seemed to be insufficient. Figure 23h shows that the entire gable wall of a masonry building almost disappeared, which probably had been cleared away after the gable wall toppled. In addition, the

roofs adopted in the buildings shown in Fig. 23f–h seemed to be simply rested on top of perimeter walls. Therefore, the roofs had no capacity of constraining out-of-plan collapse of the walls. Figure 23i illustrates that a pure sliding mode failure mechanism of a brick wall occurred at a one-story masonry building, which probably resulted from the thrust of the adjacent three-story building.

4.3 Steel buildings

Only one steel building was observed during the six-day structural seismic reconnaissance (Fig. 24a). Entry into that steel building, which is a new museum hotel with exterior circular columns and box girders (Fig. 24b, c), was not permitted. Therefore, the state of the interior structure is unknown. Once the spectral value of the experienced ground motion at the fundamental vibration period of the building surpassed the corresponding design spectral value, some damage (even minor yielding) would be expected. Nevertheless, the building seemed almost perfect (elastic) in terms of its appearance from the outside, as shown in Fig. 24a. It is thus reasonable to infer that either the spectral value did not surpass the design spectral value or some energy dissipation devices (or base isolators) were deployed in the building.

Moreover, Fig. 24 shows that the building seems to have prefabricated modules, which look like containers stacked up to three layers. Those modules are rested upon the second-floor girders. The stacked modules are covered with a roof system, which seems to consist of general metal decks, beams, and girders. Figure 24 also indicates that the long central segments of the second-floor girders are bolted to their short side segments. The short side segments of girders are then welded to columns through top and bottom circular rings. This type of beam-to-circular column connections is likely to have bolting on site and welding in factories. In addition to the better-quality control of welding in factories, the circular rings, which probably more uniformly distribute stress to the whole circumference of cross sections of columns, should be one of the factors contributing to the remarkable seismic performance of the building from the earthquake.
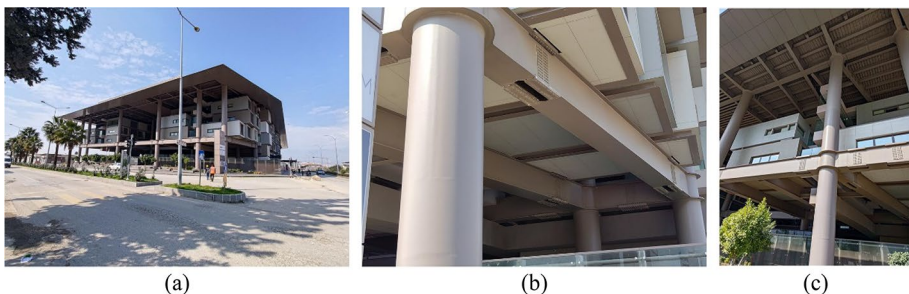

(a)   (b)   (c)

Fig. 24 **a** A steel building, **b** splices of beam segments, **c** a beam-column joint

5 Performance of bridges

5.1 Discussion of bridge structures

It is significant that thousands of buildings collapsed in southern Turkey from the sequential M_w 7.8 and M_w 7.5 earthquake events and, as far as the reconnaissance team knows, not a single bridge structure collapsed, although some were heavily damaged, which is expected and designed for in such a large event. Bridge structures have collapsed from smaller earthquakes in California than those just experienced in southern Turkey, such as from the M_w 6.6 1971 San Fernando earthquake (USGS 2021), M_w 6.9 1989 Loma Prieta earthquake (Governor's Board of Inquiry 1989), and the M_w 6.7 1994 Northridge earthquake (Seismic Advisory Board 1994). In some instances, the bridge structures that failed in past California earthquakes were over 100 miles from the epicenter. Perhaps bridges did not collapse in southern Turkey because Turkey has been keeping up with the most recent seismic bridge design specifications from California (Caltrans 2019), and elsewhere, that improve from lessons learned after each major earthquake.

While none of the bridge structures had collapsed by the time of the inspections, there are several bridges that had unusual and/or severe damage from the M_w 7.8 earthquake. Two of the bridges with the most interesting and significant observed damage are presented herein. Bridge 1 formed a column plastic hinge 25% up the column height, with vertical rebar buckling and transverse rebar yielding clearly visible, while Bridge 2 had significantly damaged girder ends, with no concrete remaining—just the rebar cage. And, yet, traffic is still flowing across both of these bridges. It is expected that multiple span collapses will happen soon at Bridge 2 from a combination of earthquake aftershocks and repeated live loading and should be closed to vehicular traffic. Bridge 1 is a major structure on a busy highway and should be assessed by the bridge design group in Turkey. Future aftershocks could cause a few more cycles and failure of the plastic hinge, resulting in complete collapse of the bridge structure. But other than some minor damage at the abutments, the rest of Bridge 1 appears to be in good condition. A seismic retrofit to the plastic hinge region, or entire column, could save this structure. Because the vertical steel has buckled, in addition to increasing the lateral confinement to the plastic hinge, new vertical steel would have to be added.

Detailed structural analyses have not been conducted for the bridge structures of interest since the bridge plans have not yet been obtained. Therefore, the presentation is of observed bridge damage and possible explanations for how the damage developed. GPS north and east coordinates, as well as elevation, were determined at the bridge sites from a Garmin 64S hand-held GPS device, allowing the closest free-field strong ground motion station to be found for each bridge, as well as the distances from the bridges to each earthquake epicenter. Bridge 1 was only 18.1 miles (29.2 km) away from the epicenter of the M_w 7.8 earthquake, while Bridge 2 was 80.8 miles (130 km) away. For the M_w 7.5 earthquake, the distances from the epicenter to the two bridges were 64.9 miles (104 km) for Bridge 1 and 134 miles (216 km) for Bridge 2. Since both bridges were significantly closer to the epicenter of the M_w 7.8 earthquake than for the M_w 7.5 earthquake, and because it was the initial, and larger, event, only the M_w 7.8 earthquake is considered in detail below.

5.2 Free-field ground motions for bridge structures

Station 2712 was the closest strong motion station to Bridge 1–2.00 miles (3.21 km) away. Free-field ground accelerations from Station 2712 during the M_w 7.8 earthquake in the horizontal east–west (EW) and north–south (NS) directions are given in Fig. 25a, b, respectively. Peak ground accelerations (PGA) are 0.607 g for the EW direction and 0.565 g in the NS direction, with PGA of 0.354 g in the vertical direction (not graphed). The 5%-damped spectral acceleration graphs for the EW and NS directions are given in Fig. 25c, with maximum values of 1.83 g and 1.90 g, respectively. Also shown in Fig. 25c is the smoothed Caltrans, 5%-damped bridge design spectral curve for a M_w 8 earthquake (plus or minus M_w 0.25) with PGA of 0.7 g and rock or stiff soil profile (Caltrans 2006), with maximum value of 1.82 g. This Caltrans design curve was obtained from an earlier version of the Caltrans Seismic Design Specifications (SDC) (Caltrans 2006) since the latest version of the SDC did not have such a graph for stiff soil and rock sites (Caltrans 2019). Station 3124 was the closest strong motion station to Bridge 2–2.14 miles (3.44 km) away. Recorded accelerations versus time at this station from the M_w 7.8 earthquake are given in Fig. 26a, b for the horizontal EW and NS directions, respectively. PGAs are 0.659 g in the EW direction and 0.581 g in the NS direction (Fig. 26a, b). In the vertical direction, the PGA was 0.589 g (not graphed). Acceleration spectrum results with 5% damping are given in Fig. 26c for the two horizontal directions. By comparing the horizontal acceleration spectra developed from ground motions measured at Station 3124 to the smoothed Caltrans bridge design acceleration spectrum for M_w 8 and PGA of 0.7 g at a rock or stiff soil site, it is clear that Station 3124 must have a deep layer of soft soil beneath it (or soft soil from the earthquake epicenter to the station) for the peak spectral responses to shift to such long natural structural periods. Therefore, Bridge 2 is probably on deep, soft soil. In the EW direction, the maximum spectral acceleration of 2.15 g (Fig. 26c) is greater than the maximum value of 1.82 g from the smoothed Caltrans design curve for M_w 8 earthquakes (Fig. 26c), demonstrating the intense level of shaking that occurred at Bridge 2.
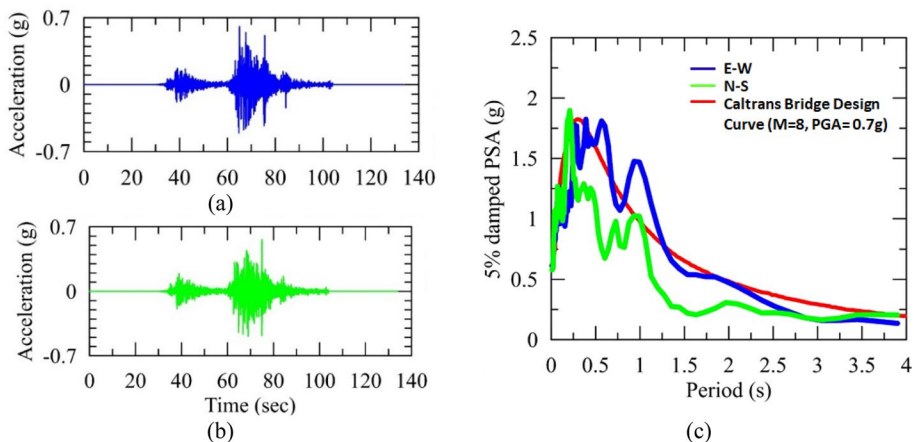

Fig. 25 Station 2712 for Bridge 1, M_w 7.8 earthquake, measured **a** EW direction accelerations versus time, **b** NS direction accelerations versus time, **c** 5% damped spectral accelerations for EW and NS directions
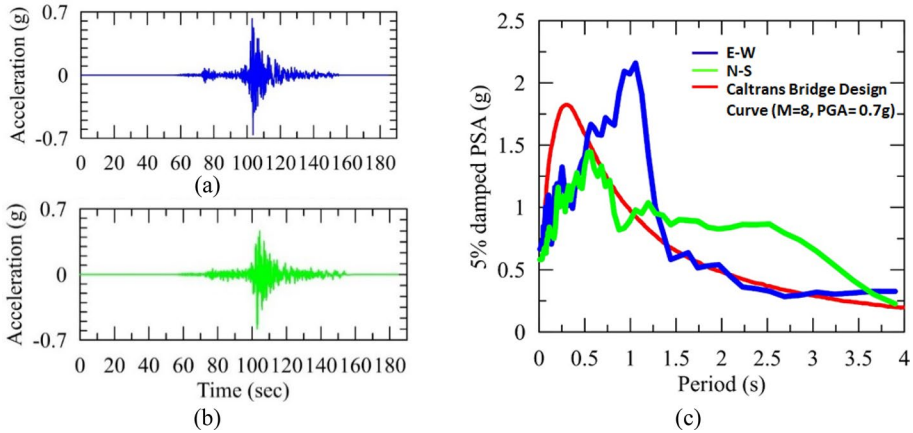
Fig. 26 Station 3124 for Bridge 2, M_w 7.8 earthquake, measured **a** EW direction accelerations versus time, **b** NS direction accelerations versus time, **c** 5% damped spectral accelerations for EW and NS directions

5.3 Observed bridge damage

Damage observed for two bridge structures is presented below.

5.3.1 Bridge 1: five span, precast, prestressed girder/steel box-girder superstructure with 10-ft-diameter RC columns

The overall impression of the side-by-side structures of Bridge 1 (Nurdag Viaduct), when looking at them from the above and adjacent roadway, is that they are large structures, with big and imposing circular columns of 10 foot (3.05 m) diameter and height of about 80 feet (24.4 m), with large, square, reinforced concrete (RC) footings (Fig. 27a). The two parallel and curved five-span bridge structures have single-column bents with RC columns, RC footings and a combination of precast, prestressed, concrete girders (Fig. 27c) and steel box girders (Fig. 27d), at GPS coordinates N 37.17096° E 36.69994° and elevation of 2563 feet (841 m). It appears that the bearings at the top of the columns may be some sort of isolation system (Fig. 27a), but the bridge plans are needed before this can be verified. Bridge 1 must have been attacked by severe ground shaking with peak spectral values in both horizontal directions exceeding the maximum Caltrans design value for a M_w 8 earthquake with PGA of 0.7 g. The Caltrans bridge design curve for M_w 8 has a scatter of plus and minus M_w 0.25, indicating that it is valid for M_w 7.75 to M_w 8.25, with the M_w 7.8 Turkey earthquake being within this range. Thus, the M_w 0.8 Caltrans seismic bridge design spectral curve is the appropriate comparison for this earthquake. While this viaduct is 18.1 miles from the epicenter of the M_W 7.8 earthquake, it was less than 0/25 miles from the fault rupture line.

A single column plastic hinge formed at these two adjacent bridge structures of Bridge 1, but not at the bottom of the column where the moment is largest for a cantilever column. The plastic hinge developed in the transverse bridge direction at about ¼ up the height of the column length (Fig. 27a). A side view of the plastic hinge region is given in Fig. 27e. On the one side of the plastic hinge, the vertical column steel buckled and the transverse
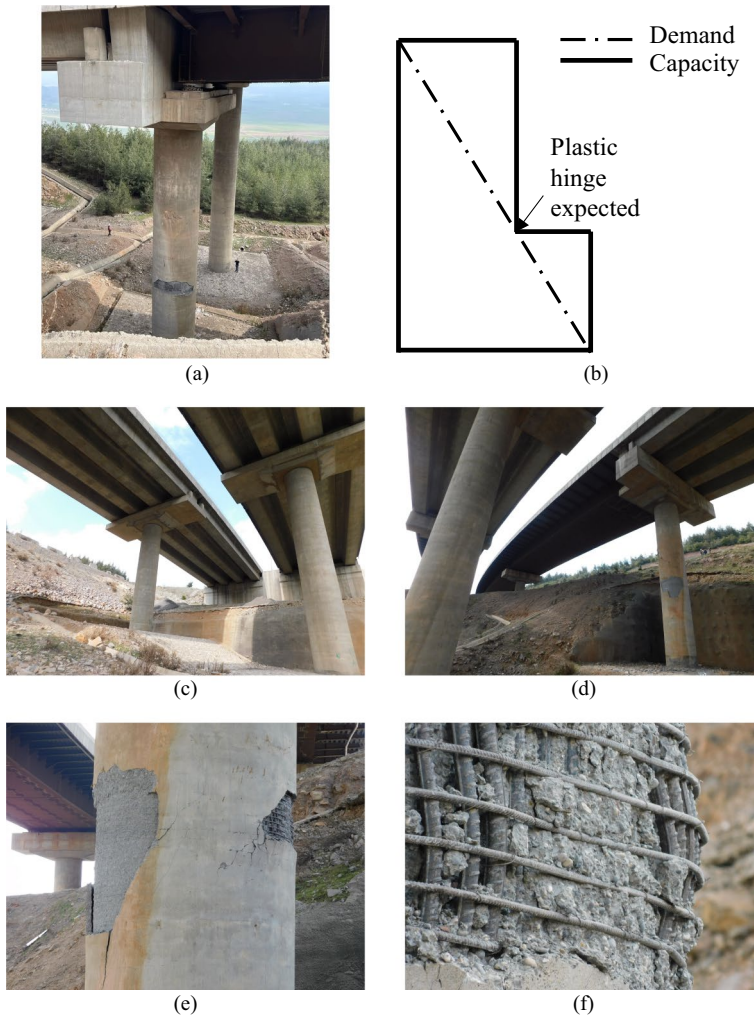
Fig. 27 Bridge 1. **a** overall view of column with plastic hinge, **b** moment demand and moment capacity of column, **c** under bridge, looking toward one abutment, **d** under bridge, looking toward other abutment, **e** Side view of column and plastic hinge, **f** plastic hinge with buckling of vertical rebar and yielding of transverse rebar

steel yielded over several rebar (Fig. 27f), while on the opposite side a large portion of cover concrete spalled off, but with no signs of transverse steel yielding or vertical rebar buckling (Fig. 27e). The most reasonable explanation for why a plastic hinge occurred 25% up the column height, instead of at the column/footing interface, as expected, is that there were vertical bar cutoffs at this location, reducing the moment capacity to the point that the moment demand/capacity ratio was larger here than at the column base (Fig. 27b). Spalling of unconfined cover concrete on both sides of this plastic hinge clearly indicates cyclic behavior in the transverse direction of the bent, with compressive concrete strains of at least 0.005 (and probably beyond 0.01) in both loading directions (Caltrans 2019, Priestley,

Calvi and Seible 1996). Vertical rebar buckling also shows that cyclic behavior occurred, as the steel must yield and reach large strains in tension before direction reversal, which results in compressive stresses and forces in the rebar before the concrete takes any significant compression from the combined section moment and axial force. This phenomenon does not occur under monotonic loading where the concrete is always in compression on one side of the neutral axis.

Vertical rebar buckling in a column plastic hinge indicates it was close to failure, suggesting that the structure was on the verge of collapse. Note that the spacing of the transverse steel looks good, but the bar size appears to be too small for a ductile plastic hinge to develop. This is probably because the plastic hinge was not expected at this location with, perhaps, larger transverse rebar provided towards the bottom of the column. While bar cutoffs is the most likely reason a plastic hinge formed part way up the column height, it is possible that this location had a larger moment demand than at the base of the column due to the combined effects of the transverse mass and rotational mass inertia from the large bridge structure, which is especially important for single-column-bent bridges (Dowell 2004) since the bridge is free to rotate at the top in the transverse direction as it displaces.

5.3.2 Bridge 2: six span, precast, prestressed, I-girder superstructure with RC columns

These two parallel and straight bridges (Asi Bridge) are over water (Asi River) and located at GPS coordinates N 36.25505° E 36.20430° and elevation of 315 feet (96.0 m). They consist of precast, prestressed, I-girders with RC topping slab and CIP columns (Fig. 28a). Lateral motion of the bridge caused severe damage and failure of external shear keys (Fig. 28b). The ends of all of the precast concrete girders were extensively damaged at the abutments from large vertical accelerations and forces, including impact, resulting in shear cracks and extensive spalling of the concrete, as shown in Fig. 28c, d. The spalling extended a long distance out into the girder (Fig. 28c), far beyond the supports. In many cases, there was no concrete left, with just the rebar cage remaining toward the girder end (Fig. 28d).

This brings up an interesting question as to what happened to the prestressing strands and associated prestressing force, as the concrete around the strands spalled out. A coiled-up prestressing strand was found adjacent to one of the bridge abutments that had flown out of a girder. The extensive damage to the ends of internal and external girders appears to be a result of a sequence of events; first diagonal shear cracks form just beyond the supports from large vertical accelerations and forces, including impact from girder-end liftoff and slamming back down (peak vertical spectral acceleration of 1.64 g), then concrete begins to spall off at the girder ends due to the combined effects of large vertical, transverse and longitudinal forces, including impact in all three directions. Also, vertical rebar in the girder web buckled out, pushing concrete off in both directions, which contribute to the damage at the girder ends and the extensive length of this region.

With no concrete left at the girder ends, there is nothing to hold the prestressing steel to the girder end region, with the transfer length moving to where there is still concrete, causing added damage to the already-cracked girder end region, with more spalling and slip, until a much longer distance of damage has developed than from just diagonal shear cracking. As seen in Fig. 28c, the spalled region at the girder ends is very long. Severe twisting and bending of one precast girder occurred, as seen in Fig. 28e, f. Also, plastic hinges developed at the base of the columns in the longitudinal direction, as expected. Settlement occurred at both approaches to the bridge, requiring vehicles to slow down to enter and exit the structure.

Fig. 28 Bridge 2. **a** overall view from underneath the bridge, **b** failed exterior shear keys, **c** damage at girder ends, **d** concrete damage and spalling at girder ends, **e** damaged and twisted girder end, **f** bent girder

However, traffic should not be allowed on this bridge as it is just a matter of time before complete span collapses occur from continued traffic loading and/or earthquake aftershocks. The Asi Bridge was 80.8 miles from the epicenter, but only 2.5 miles from the fault line, which demonstrates that the distance to the fault rapture is also important than to the epicenter, based on the intense level of shaking and damage at this bridge.

6 Performance of industrial buildings

6.1 Precast concrete buildings

In Turkey, industrial buildings are predominantly constructed RC precast structures. This type of building system offers numerous benefits, including speedy construction, lower project costs due to prefabrication, adherence to high-quality standards, and improved safety. However, the statically determinate scheme commonly used in this type of construction is considered its most significant drawback. For single-story industrial buildings in Turkey, precast reinforced concrete long-span roof girders are supported by cantilever precast columns, which allow for large, open spaces necessary for manufacturing (Saatcioglu et al. 2001). This is the most frequently used typology for this type of construction, and it was also observed in the Turkoglu Organized Industrial Zone (OIZ).

The typical major direction of the structures investigated in the Turkoglu OIZ in Kahramanmaras had spans of roughly 15 m to 25 m, and the other direction had spans of approximately 8 m. Their story heights ranged from 7 to 10 m (Figs. 29a, 30a). As illustrated in Fig. 29a, the base of each precast column was grouted into a precast pocket foundation to make a fixed connection, and some of the column ends formed plastic hinges, as shown in Fig. 29b. The long-span roof girders were positioned along the building's transverse axis and were simply supported by column corbels. The depth of these girders frequently changes over their length, resulting in a triangle configuration (double-slope girders). Beams are directed along the building's longitudinal axis. Purlins span at regular intervals between the roof girders. The prefabricated roof girders, gutter beams, and purlins were simply held together at both ends (Fig. 29b, c). The horizontal beam–column connection is
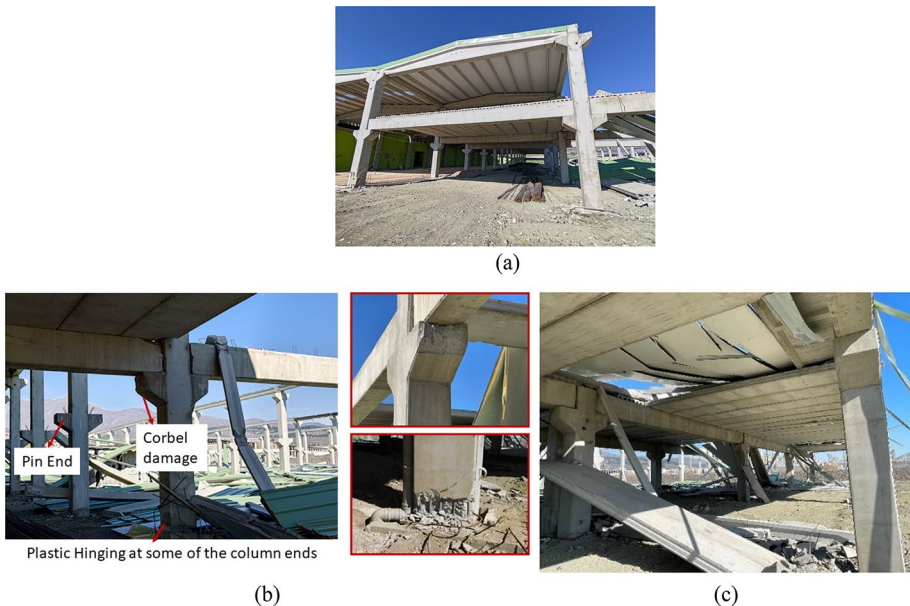

(a)

Pin End

Corbel damage

Plastic Hinging at some of the column ends

(b)

(c)

Fig. 29 Damage of precast building: **a** undamaged portion of the precast building, **b** corbel damage and plastic hinging of column, **c** precast slab failure

(a)   (b)

Fig. 30 Damage of precast buildings in Turkoglu OIZ **a** precast tapered beam failure owing to the loss of support, **b** cladding panels due to panel-to-structure failure

built by seating the beams on the column capitals and keeping the beam ends in place with vertical steel dowels, as shown in Fig. 29b. The industrial building that was under construction collapsed due to unseating of the girder ends or from the beams rotating over. Because the first portion of the structure operated successfully, as shown in Fig. 29a, the failure was considered to have started at the pin connections, which were not correctly knotted since they were still under construction. The roof was constructed out of lightweight materials, which does not act as a structurally robust diaphragm and permits the girders to flip out of plane. Furthermore, as indicated in Fig. 30b, precast concrete wall panels were commonly employed for the external walls of Turkoglu OIZ. The connection details for the wall panels are normally designed so that the panels do not contribute to the lateral stiffness of the building; however, the existing industrial precast concrete buildings in the affected area did not meet this principle, resulting in detachment of the exterior cladding elements as shown in Fig. 30b.

6.2 Reinforced concrete buildings

Three reinforced concrete industrial buildings were investigated during the six-day structural seismic reconnaissance (Fig. 31). Entries into the buildings were not permitted. Therefore, the state of the interior structures is unknown. Figure 31a shows a damaged reinforced concrete building (Coordinates: 37.45764°N, 37.25636°E) due to joint failure. It was built before 2000, and no deaths were reported. Reinforcement detailing is important to provide continuity across the joint, so a lack of reinforcement can cause unexpected stress concentrations that lead to cracking and failure. The figures indicate rebar slipping, which might occur due to insufficient reinforcement development length, which is required to transfer the loads to the concrete. Another factor that might lead to this failure is the quality of materials used. Figure 31b, c shows similar damaged reinforced concrete buildings due to the large mass at the roof. They were built before 2000, and no deaths were reported (Coordinates: 37.19352°N–036.57438°E) for Fig. 31b and (Coordinates: 36.59820°N–36.19591°E) for Fig. 31c. Damage observed in these buildings was due to a storage tank/mass on the roof. The reason for the fall-over might be high vertical acceleration observed from the earthquake, which causes extra weight of the storage tank due to the vertical component of the earthquake. It may not have been taken into account during the design process. On the other hand, the inertial forces at the top part of buildings due to amplification of the horizontal component of the earthquakes are higher than
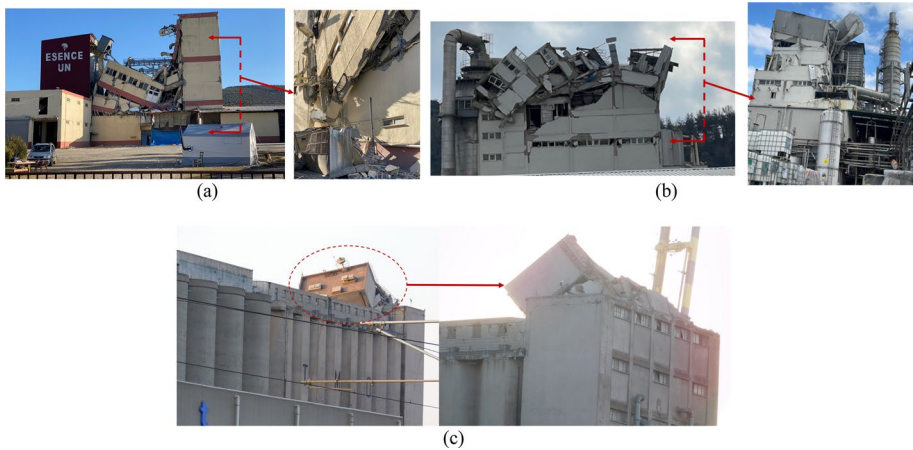
Fig. 31 Damage of RC buildings **a–b** Essence Un, **c** and **d** ABC Deterjan, **e** Toprak Mahsulleri Ofisi (TMO)

at the lower stories. High lateral acceleration demand at the top might have caused shear connection failure.

6.3 Steel structures

Full steel structures are not commonly used in Turkey. Instead, a combination of steel members with reinforced concrete or precast frames is generally used for industrial structures. During the reconnaissance, only two buildings constructed with a combination of concrete and steel were found. The first structure was under construction at the time of the earthquake in Turkoglu OIZ [Coordinates: 37.33625°N and 36.81581°E]. As illustrated in Fig. 32a, the gravity-load framing system of this construction consists of a steel space frame, which is supported by steel trusses that span between reinforced concrete columns. For the extension of corbels, short steel columns were utilized on top of the reinforced columns. This type of structure is rather widespread in Turkoglu OIZ. Overall, the roof frame behaved well; nevertheless, tilting of the steel truss beams was noted, as shown in Fig. 32b. The light roof covers that were temporarily attached to the roof collapsed, causing buckling at one of the bracings (Fig. 32c).

Another hybrid structure is owned by Iskur and located in Kahramanmaras (Fig. 33a, Coordinates: 37.55340°N and 36.96157°E]. One of the factory's buildings was exposed to multi-hazard, as shown in Fig. 33b. The factory was not damaged structurally by the earthquake; however, a spark at the generator during the earthquake created a fire, which quickly became uncontrollable due to the extremely combustible materials they were using. When the steel temperature rises, corrosion, dimensional changes, and permanent changes in the steel microstructure occur, resulting in a reduction in steel modulus of elasticity and strength, and ultimate collapse of the structure (Fig. 33c).

6.4 Silos

Silos are used to store a wide range of goods between supply and demand. Failure of these structures could disrupt the food chain or cause collateral damage including fires,
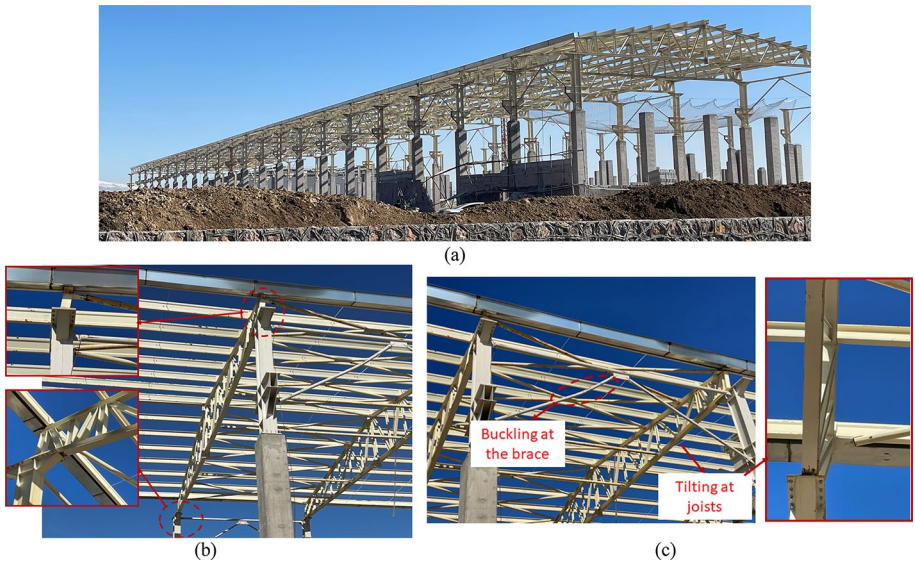
Fig. 32 Damage of steel roof system including reinforced concrete columns **a** overall view of structure, **b** steel truss tilting, **c** buckling at the brace due to collapsing of light roof covers

Fig. 33 Multi-hazard on steel suspended ceiling structural system **a** prior to earthquake, **b** after the earthquake and fire, **c** detailing

explosions, and the release of hazardous substances into the air or soil. As a result, understanding the behavior of these structures when subjected to seismic loads is crucial. An earthquake ground motion contains three components that result in structural loads in three directions: vertical, and two horizontal. Vertical seismic loads have a minor impact on relatively heavy silo structures; however, lateral loads can significantly impact taller silos storing heavier contents. The magnitude of the horizontal seismic load is related to the silo's weight. The height of the silo structure's center of mass rises as the height of the silo rises. Considering that the horizontal seismic load is applied nearly at the center of mass, the moment arm for the lateral load and the associated moment at the base increases. The higher moment causes a nonuniform pressure distribution at the base of the silos, which can be substantially more critical than the pressure induced by gravity loads. Figure 34a shows significant buckling at the bottom end of the silos and failure of arches. If the flow parameters of the bulk material being handled in a silo differ from, or have greater changes than, those for which the silo was intended, obstructions such as arches and ratholes may form, and the flow pattern and loads may be entirely different than anticipated (Carlson and Holmes 2003). Many steel silos in the Nurdagi region were subjected to elevator failure, as shown in Fig. 34a, which caused dynamic loading to silos that lead to total or partial collapse of the structure. Smaller, elevated, cylindrical metal silos are often supported on local brackets attached to the side of a shell (Doerich and Rotter 2008), which causes linear-elastic deformations and bifurcations. Figure 34b shows the deformation at the supporting system of a small metal silo. One of the metal silos totally collapsed due to the overturning moment of the structure while the other one formed flexural buckling at the supporting system. Brittle welded connection failure was observed at the supporting system of the metal silo. Damage to the concrete silo was concentrated in the walls near the bottom of the silos

Fig. 34 Damage of silos **a** corn silos, **b** total collapse of a slender metal silo due to brittle welded connection, **c** concrete spalling on silos

Fig. 35 Performance of schools in Iskenderun **a** Pre-school, **b** Retrofitted elementary school, **c** Unretrofitted elementary school

as shown in Fig. 34c. Severe concrete crushing, lack of sufficient reinforcement, steel bar fractures and buckling were observed.

7 Critical facilities

7.1 Schools

In Turkey, a national policy is in place to mitigate earthquake impacts and enhance preparedness at national, regional, local, workplace and family levels. This includes pre-earthquake inspection of critical infrastructure (i.e., schools and public buildings) and prioritization for strengthening based on relative risk scoring. School buildings in Golbasi and Iskenderun, where liquefaction is the main problem in the region, were investigated. Settlements in a garden wall [Fig. 35a, Coordinates: 36.59325°N and 36.16602°E], damage to nonstructural elements, such as infill walls [Fig. 35b, Coordinates: 36.55244°N and 36.15448°E], as well as heavy equipment movement that was observed on several occasions, pose a threat, particularly in schools, for the lives of students. Fortunately, schools were just recently closed at the time of the earthquake;

however, the observations above highlight the necessity of pre-earthquake assessment of potential nonstructural damage and the need for mitigation measures. According to the president of Dr. Gani Bahadirli Elementary School, most schools in the Iskenderun area had been seismically retrofitted in the previous 7 years. As a result, the majority of schools in the region suffered limited, to no, damage. Those that had not yet been retrofitted suffered severe damage, such as the collapse of the conference room in the additional building of Mithatpasa Primary School, as depicted in Fig. 35c (Coordinates: 36.59121°N and 36.16785°E).

7.2 Places of worship (mosques and churches)

Worship structures are significant because they have the capacity to accommodate large groups of people who need to stay safe and warm after an earthquake. As a result, their performance is critical not only during an earthquake, but also after earthquakes to ensure that operations continue uninterrupted. In numerous occasions, in the Kahramanmaras and Osmaniye regions, the most vulnerable part of a mosque was the minaret, which toppled over, while the rest of the mosque was not affected. The minaret is attached to the mosque at the second story level, with stiffness and boundary variation in the height, resulting in cracks, typically at areas with abrupt cross-sectional changes, which causes the minarets to fall. Figure 36a illustrates the partial collapse of the minaret from where this cross-sectional change begins. Serious damage and the failure of the mosque was found in Golbasi and Iskenderun, where settling was the primary cause. When soil supporting foundations is subjected to excitation during an earthquake, it may experience consolidation or shear failure, resulting in ground settlement or subsidence. Ground settlement can cause buildings to shift, resulting in masonry wall damage, as demonstrated in Figs. 36b, 37 for a mosque and church, respectively. According to locals, the dome of St. Ilyas church (Coordinates: 36.09764°N and 35.99159°E) suffered moderate damage after the main shock and collapsed following the Samandagi earthquake [February 20, 2023, see Fig. 37a].

7.3 Hospitals

Following a major earthquake, emergency management is crucial in limiting the disaster's impact. Hospital infrastructure, road viability, search and rescue teams, civil protection activities, helicopter medical evacuations and, most importantly, field hospital facilities all play a role in emergency management. Several components of response management are interconnected. As a result, during a crisis, all components must work efficiently and effectively while considering the consequences of the others. As the primary component of emergency management, hospitals should be designed to handle large numbers of victims during and after natural disasters. Hospitals in Kahramanmaras and Iskenderun were checked, and it was discovered that a couple of old state hospitals were moderately damaged during the two large earthquakes on February 6th, forcing the hospital to evacuate following the incident (Fig. 38a). In the preceding decade, the General Directorate of Health Investments of the Ministry of Health chose to develop new city hospitals with seismic base isolators to limit earthquake damage in high seismic zones. Figure 38b depicts a lead rubber bearing seismic isolator used in the Malatya City Hospital addition. During the earthquake, the existing major part of Malatya City hospital performed admirably.

(a)

(b)

Fig. 36 Damage of mosques **a** Haci Murat Mosque in Kahramanmaras, **b** Merkez Cumhuriyet Mosque in Pazarcik

8 Discussion and conclusions

On February 6, 2023, a sequence of earthquakes with magnitudes of M_w 7.8 and M_w 7.5 struck Kahramanmaras and affected a total of ten different cities with a total of 15 million people. The reconnaissance team spent a total of two weeks in the field inspecting structural and geotechnical damage, starting one week after the main shock. The team visited Iskenderun, Antakya, Osmaniye, Kahramanmaras, Gaziantep, Nurdagi, and Golbasi. Disparities between the seismic code requirements and the design/construction practices of the damaged buildings were primarily responsible for the structural damage observed in the inspected structures. The buildings that sustained damage were found to have been constructed using in situ mixed concrete with low strength (i.e., 6–10 MPa). Poor workmanship and a lack of oversight during the construction process likely led to construction practice issues that resulted in extensive damage to RC residential

Fig. 37 Damage of churches **a** St. Ilyas church in Samandagi, Antakya, **b** Roman Catholic Church in Iskenderun
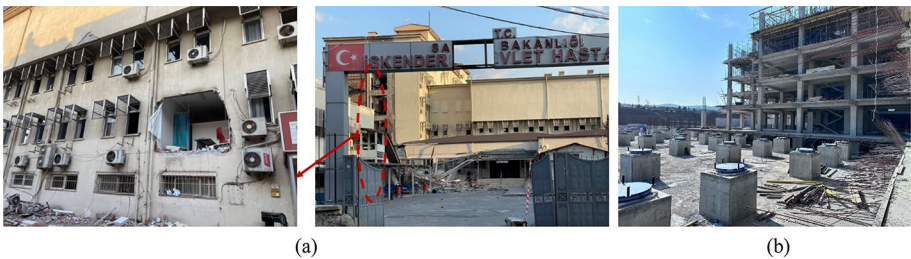
Fig. 38 Hospitals **a** old state hospital in Iskenderun, **b** New city hospital in Malatya

buildings. Several common observations were made in many older buildings, including stirrups bent with 90-degree hooks, unengaged stirrups, large stirrup spacing, and the absence of cross ties.

These improper details not only jeopardize the section's integrity but also result in shear failure and limited ductility capacity of RC members, as observed in previous catastrophic events in Turkey (Akansel and Ozkula 2021). Most residential building failures, and related deaths, occurred in a particular type of construction that is used throughout Turkey consisting of a RC frame of columns and girders, and infill walls of bricks or masonry blocks, with no gaps between the walls and the frame. The infill walls are not connected to the frame members, and the bricks, or masonry blocks, are not tied to each other. Because of this, the infill walls are not considered in seismic design as part of the lateral load-resisting system. However, as the diagonal shear cracks seen by the reconnaissance team on almost all infill walls for most of these buildings clearly demonstrate, these walls are resisting lateral loads before they fail and (partially or fully) fall out, forcing the RC frame to suddenly take all of the earthquake loads. The combined response of the frame and infill walls is much stiffer than the frame acting by itself, causing amplification of the earthquake loads above what is considered in the design, leading to the failure of these building types. Infill walls can also cause a short column effect, with larger shears than expected from the full column assumption. In addition, many building failures were also due to soft soil and liquefaction of sandy

soils, and related settlement, with some building structures rotating as a unit about their foundations. Sand boils, liquefaction, lateral spreading, settlement and multiple wide-open, deep cracks in the soil were seen in several locations.

While thousands of residential buildings collapsed, as did various mosques, churches, silos and industrial buildings, there were no bridge failures as far as the reconnaissance team is aware. Several bridge structures had severe damage, as expected under such an extreme event, but they remained standing. This demonstrates that it is possible to design and build civil engineering structures that do not collapse from large earthquakes. While RC buildings with infill walls failed in almost unbelievable numbers, some were heavily damaged but remained standing, with girder and column plastic hinges in critical locations properly forming. Prior to rebuilding, it is recommended to consider changes to this type of building structure. If a similar type of building is used, infill walls must be connected to the frame members and a gap provided to allow the columns and girders to bend and form plastic hinges where they are designed and detailed to occur for seismic loading. Bricks and masonry blocks must also be connected to each other to prevent them from falling to the street below or into the apartments. The geotechnical engineering reconnaissance highlights the necessity of (1) further investigating the widespread liquefaction that occurred in Iskenderun; (2) systematic monitoring of the earth dams to identify the mechanisms that played a role in those damaged during the earthquakes, and those that performed well; and (3) investigation of the slope instability in Altinozu, Hatay, for progressive failure potential; and (4) site amplifications in various districts. Moreover, the exceedance of the TEBC (2019) design spectrum for the return period of 2475 years by response spectra of recorded motions at aforementioned stations should be further assessed in future studies.

References

ACI 318 (2005) Building code requirements for structural concrete (ACI 318-05) and commentary (ACI 318R-05), ACI Committee 318, American Concrete Institute, Farmington Hills, MI

Akansel VH, Ozkula G (2021) The 30 october 2020, Mw 6.6 sisam (Samos) earthquake: interpretation of strong ground motions and pos-earthquake condition of nearby structures. Eur J Eng Appl Sci 4(2):66–86

Akkar S, Boore DM (2009) On baseline corrections and uncertainty in response spectra for baseline variations commonly encountered in digital accelerograph records. Bull Seismol Soc Am 99(3):1671–1690

Caltrans Seismic Design Criteria (SDC) (2006) Version 1.4.

Caltrans Seismic Design Criteria (SDC) (2019) Version 2.0

Carlson JW, Holmes T (2003) Silo failures: Why do they happen? TASK q 7:499–512

Cetin H, Güneyli H, Mayer L (2003) Paleoseismology of the Palu-Lake Hazar segment of the East Anatolian fault zone Turkey. Tectonophysics 374(3–4):163–197

Cetin KO, Ilgac M, Can G, Cakir E (2023) Preliminary reconnaissance report on February 6, 2023, Pazarcık M_w=7.7 and Elbistan M_w =7.6, Kahramanmaraş-Türkiye Earthquakes. METU Earthquake Engineering Research Center

Competing Against Time: Report to Governor Deukmejian from the Governor's Board of Inquiry on the (1989) Loma Prieta earthquake, 1989.

Converse AM, Brady AG (1992) Basic strong-motion accelerogram processing software version 1.0

Doerich C, Rotter JM (2008) Behavior of cylindrical steel shells supported on local brackets. J Struct Eng 134:1269–1277

Dowell RK (2004) Time-history analysis vsersus measured seismic responses of the 5/14 connector bridge, Report (#DH-04-02) to the strong motion instrumentation program, California Geological Survey, from Dowell-Holombo Engineering, 2004)

Hancilar U, Sesetyan K, Cakti E, Safak E, Yenihayat N, Malcioglu FS, Donmez K, Tetik T, Suleyman H (2023) Kahramanmaraş-Gaziantep Türkiye M7.7 Earthquake, 6 February 2023 (04:17 GMT+03:00) Strong Ground Motion and Building Damage Estimations Preliminary Report (v6)

Hashash YMA, Musgrove MI, Harmon JA, Ilhan O, Xing G, Numanoglu O, Park D (2020) DEEPSOIL 7.0, user manual. Board of Trustees of University of Illinois at Urbana-Champaign. Urbana

Lin JL, Kuo CH, Chang YW, Chao SH, Li YA, Shen WC, Yu CH, Yang CY, Lin FR, Hung HH, Chen CC, Su CK, Hsu SY, Lu CC, Chung LL, Hwang SJ (2020) Reconnaissance and learning after the february 6, 2018, earthquake in Hualien, Taiwan. Bull Earthq Eng 18(10):4725–4754

Ministry of Environment and Urbanization of Turkey (2023) https://hasartespit.csb.gov.tr/

Priestley MJN, Seible F, Calvi GM (1996) Seismic design and retrofit of bridges. John Wiley and Sons, New York

Saatcioglu M et al (2001) The August 17, 1999 Kocaeli (Turkey) earthquake–Damage to structures. Can J Civ Eng 28(4):715–773

Seed HB, Romo MP, Sun JI, Jaime A, Lysmer J (1988) The Mexico earthquake of september 19, 1985—relationships between soil conditions and earthquake ground motions. Earthq Spectra 4(4):687–729

Seismic Advisory Board (1994) The continuing challenge: report on the northridge earthquake to the director. Department of Transportation, State of California

Selcuk (1985) Kızıldağ–Keldağ–Hatay dolayının Jeolojisi ve Jeodinamik evrimi, M.T.A Rapor No 7787, Ankara. (in Turkish)

Şeşetyan K, Stucchi M, Castelli V, Gómez Capera AA (2023) Kahramanmaraş-Gaziantep Türkiye M7. 7 Earthquake, 6 February 2023 (04: 17 GMT+ 03: 00) Large historical earthquakes of the earthquake-affected region: a preliminary report

Taskesen-Ozturk G (2018) Analysis of spatio-temporal changes of precipitation to estimate R factor in RUSLE at Kartalkaya Dam. MSc Thesis, Middle East Techncial University, Ankara, Turkey. p 84

TEBC (2019) Turkish building earthquake code; T.C. Resmi Gazete: Ankara, Turkey

USGS (2021) 50 Years later, an earthquake's legacy continues. Disaster that helped nation prepare for future earthquakes: remembering the San Fernando. Retrieved from https://www.usgs.gov/news/featured-story/disaster-helped-nation-prepare-future-earthquakes-remembering-san-fernando#:~:text=The%20San%20Fernando%20earthquake%20struck,risks%20and%20bolster%20public%20safety

USGS (2023a) https://earthquake.usgs.gov/earthquakes/eventpage/us6000jllz/executive

USCS (2023b) https://earthquake.usgs.gov/earthquakes/eventpage/us6000jlqa/executive

Yuksel A, Gundogan R, Akay AE (2008) Using the remote sensing and gis technology for erosion risk mapping of Kartalkaya dam watershed in kahramanmaras, Turkey. Sensors 8(8):4851–4865

Authors and Affiliations

Gulen Ozkula[1] **· Robert K. Dowell[2] · Tugce Baser[3] · Jui-Liang Lin[4] ·**
Ozgun A. Numanoglu[5] · Okan Ilhan[6] · C. Guney Olgun[7] · Cheng-Wei Huang[4] ·
Tunc Deniz Uludag[8]

✉ Gulen Ozkula
   ozkulag@uwplatt.edu

[1] Department of Civil and Environmental Engineering, University of Wisconsin, Platteville, WI 53818, USA

[2] Department of Civil, Construction, and Environmental Engineering, San Diego State University, San Diego, CA 92182, USA

[3] Department of Civil and Environmental Engineering, University of Illinois at Urbana Champaign, Champaign, IL, USA

[4] National Center for Research on Earthquake Engineering, Taipei, Taiwan

[5] Schnabel Engineering, Seattle, WA 98188, USA

[6] Department of Civil Engineering, Ankara Yildirim Beyazit University, Ankara, Turkey

[7] Department of Civil, Architectural and Environmental Engineering, Missouri University of Science and Technology, Rolla, MO 65409, USA

[8] Martin/Martin Engineering, Denver, Fort Collins, CO 80525, USA